Influences of various orifice layouts on the properties of aerostatic journal bearings based on finite element method

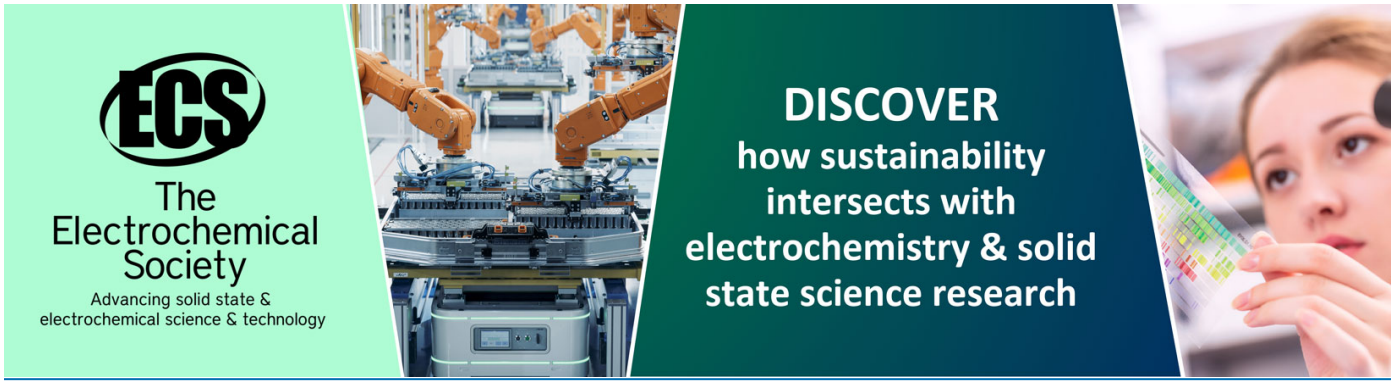

IOP Conf. Series: Materials Science and Engineering **657** (2019) 012044 doi:10.1088/1757-899X/657/1/012044

Influences of various orifice layouts on the properties of aerostatic journal bearings based on finite element method

S Y Gao[1,2,5], Y G Shi[2], S Yang[2,3], P Sun[2] and T J Li[4,5]

[1]The State Key Laboratory of Mechanical Transmissions, Chongqing University, 400044, Chongqing, PR China
[2]Institute of Advanced Manufacturing Technology, Hefei Institutes of Physical Science, Chinese Academy of Sciences, Changzhou, 213164, Jiangsu, PR China
[3]State Key Lab of Digital Manufacturing Equipment and Technology, Wuhan, 430074, Hubei, PR China
[4]School of Mechanical Engineering, Shanghai University of Technology, Shanghai 200093, PR China

E-mail: sygao@iamt.ac.cn/litianjian99@163.com

Abstract. It is essential to thoroughly investigate influences of orifice layouts on properties of aerostatic journal bearings employed in ultra-high speed spindles. In this paper, four orifice layouts of aerostatic journal bearings which have a large length-diameter ratio are designed and investigated, particularly in light of the nonlinear compressible Reynolds equation and the associated computational analysis and algorithms using the FEM-based Galerkin weighted residual method. A series of pressure distributions as well as the load capacity, attitude angle, volume flow rate and air film stiffness of the aerostatic journal bearings for the cases of four orifice layouts are analysed with respect to different rotational speeds and eccentricity ratios. It can be concluded that increasing orifice sets is not beneficial to enhance the performance of the aerostatic journal bearing. The aerostatic journal bearing divided into two identical independent aerostatic journal bearings has relative optimal performance at rotational speeds from 0 r/min to 160,000 r/min, such as the highest load capacity, the lowest attitude angle and modest air film stiffness, however, with consumption of the largest quantities of pressurized gas. The designers can use the analysis results to optimize the orifice layout for improving the performance of the aerostatic journal bearing.

1. Introduction

Air bearings have outstanding features of almost zero friction, clean and high supporting accuracy with respect to ball bearings [1,2]. Hence, air bearings become the essential components of high speed motorized spindles which are commonly used in precision micro-machining fields with the top speed of greater than 100,000 r/min [3,4]. Aerostatic bearings, one type of air bearings, have many types of restrictors, such as porous restrictor, slot restrictor, orifice restrictor and so on. However, orifice restrictors play a dominant role in the academic and industrial communities. It is of great significance to study the varied properties of aerostatic bearings influenced by orifice layouts for developing higher accuracy bearings which are employed to the ultra-precision aerostatic spindles.

Large quantity of research papers had been reported to investigate properties of the aerostatic bearing by numerically solving the Reynolds equation with finite difference method (FDM) or finite element method (FEM). Gas film pressure and load capacity of the aerostatic bearing with a length-

diameter ratio of 1 were analysed based on the modified Reynolds equation [5]. Rotation effects of hybrid air journal bearings were studied by numerically solving the Reynolds equation with FDM [6]. Effects of the geometrical and running parameters on the characteristics of the micro air journal bearing were obtained by applying the Newton iteration and the FDM to analyse the Reynolds equation [7]. Aerodynamic and aerostatic effects of aerostatic bearings were investigated through numerically calculating the Reynolds equation associated with the Newton's method [8]. The Reynolds equation was numerically analysed by FDM and successive over-relaxation (SOR) method to calculate the load capacity and stiffness of air bearings [9]. Air film pressures of aerostatic bearings were analysed with Euler explicit approach and central FDM [10,11]. Besides, air film pressures and stiffnesses of aerostatic journal and thrust bearings were studied based on the FDM and the successive relaxation method [12]. Furthermore, the Reynolds equation was numerically calculated by FEM to study the radial load capacity and air film stiffness of the air spherical bearing [13], and the effects of pressure-equalizing grooves of aerostatic journal bearings were also investigated [14]. The Reynolds equation with the velocity item was further discretized by FEM to study the performance characteristics of the aerostatic journal bearing under conditions of ultra-high speeds and eccentricities [15]. Based on the aforementioned analyses, the performance investigations of the aerostatic bearings were conducted in many papers, however, most of the length-diameter ratios of the aforementioned aerostatic journal bearings were less than 2, and few research literatures were published to discuss the influences of orifice layouts on the properties of aerostatic journal bearings which have a large length-diameter ratio. Therefore, in this study, influences of various orifice layouts on the properties of the aerostatic journal bearings with a large length-diameter ratio are investigated by numerically solving the nonlinear compressible Reynolds equation based on the FEM.

2. Aerostatic journal bearings with various orifice layouts

Figure 1 shows the designed four orifice layouts of the aerostatic journal bearing. Different orifice sets are designed in each bearing and twelve equispaced orifices are distributed in each orifice set. The bearing length, L, is 60 mm, the bearing bore diameter, D, is 20 mm, the orifice diameter, d, is 0.2 mm, the gas film thickness without eccentricity, h_n, is 20 μm, the supply gas pressure, p_s, is 0.7 MPa. Section a-a is the axial middle plane of the aerostatic journal bearing.

Case 1: two orifice sets are symmetrical with respect to the section a-a, and l/L=1/5.

Case 2: four orifice sets are symmetrical with respect to the section a-a, and $l_1/(L/2)$=1/5, $l_2/(L/2)$=4/5.

Case 3: four orifice sets are symmetrical with respect to the section a-a. There is an exhaust vent in the axial middle position of the bearing. Thus, the whole bearing is divided into two identical independent small aerostatic journal bearings and the section b-b is the axial middle plane of the small aerostatic journal bearing. Two orifice sets are symmetrical with respect to the section b-b. The axial length of the small aerostatic journal bearing is $L/2$, and $l_3/(L/2)$=1/5.

Case 4: six orifice sets are symmetrical with respect to the section a-a, and l_4/L=1/10, l_5/L=1/4, l_6/L=2/5.

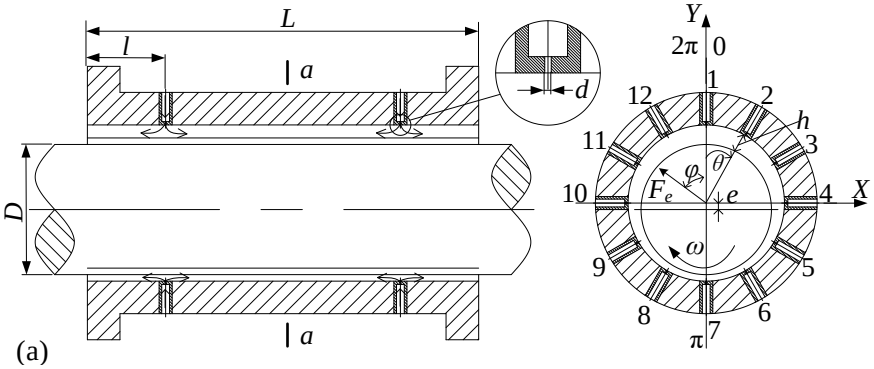

(a)

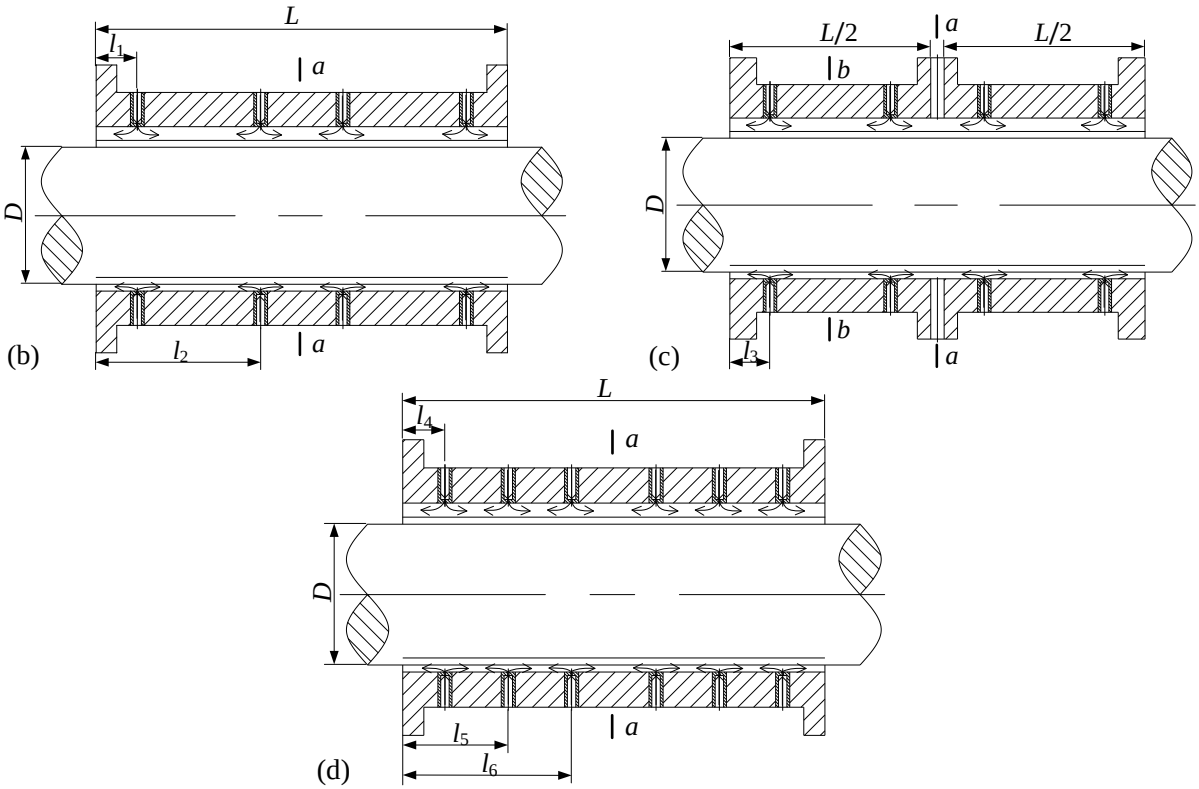

Figure 1. Four orifice layouts of the aerostatic journal bearing. (a) Case 1. (b) Case 2. (c) Case 3. (d) Case 4.

3. Computational model

3.1. Governing equations

The dimensionless Reynolds equation is depicted in equation (1) [15,16]

$$\frac{\partial}{\partial \bar{x}}\left(\bar{h}^3\frac{\partial \bar{p}^2}{\partial \bar{x}}\right)+\frac{\partial}{\partial \bar{z}}\left(\bar{h}^3\frac{\partial \bar{p}^2}{\partial \bar{z}}\right)=\Lambda_x\frac{\partial\left(\bar{h}\bar{p}\right)}{\partial \bar{x}}+\Lambda_z\frac{\partial\left(\bar{h}\bar{p}\right)}{\partial \bar{z}} \tag{1}$$

where Λ_x and Λ_z are dimensionless bearing numbers, $\bar{x}$ and $\bar{z}$ are dimensionless Cartesian coordinates, $\bar{h}$ is the dimensionless thickness, $\bar{p}$ is the dimensionless pressure.

In this study, the dimensionless Reynolds equation has the following boundary conditions.

- Pressure at the outer border of the bearing: $p=p_a$, p_a is ambient pressure;
- Pressure at the symmetric boundary: $\frac{\partial p}{\partial n}=0$, n is the normal direction of the symmetric boundary;
- Pressure at the orifice boundary: $p=p_r$, p_r is the pressure at the orifice outlet.

The numerical solution of the Reynolds equation is calculated by FEM with the triangular element, and the finite element formula of the Reynolds equation is deduced as follows

$$\sum_{e\in\Delta i}\int_{\Delta e}\left(\mathbf{N}^{eT}\mathbf{h}^{e}\right)^{3}d\bar{x}d\bar{z}\left(c_i\mathbf{c}^{eT}+b_i\mathbf{b}^{eT}\right)\mathbf{f}^{e}\frac{1}{\left(2\Delta e\right)^{2}}-\bar{Q}\zeta_i$$
$$-\sum_{e\in\Delta i}\lambda\left(c_i\bar{u}+b_i\bar{\omega}\right)\mathbf{h}^{eT}\int_{\Delta e}\mathbf{N}^{e}\mathbf{N}^{eT}d\bar{x}d\bar{z}\frac{1}{2\Delta e}\left(\mathbf{f}^{1/2}\right)^{e}=0 \quad (2)$$
$$\left(i=1,2,\ldots,q\right)$$

where $\mathbf{N}^e$ is the shape function, $\mathbf{h}^e$ is the column matrix of the node thickness, c_i and b_i are the coefficients of the interpolation function, $\mathbf{c}^e$ and $\mathbf{b}^e$ are the coefficient matrixes of the interpolation function, $\mathbf{f}^e$ is the column matrix of dimensionless node pressure square, $\bar{Q}$ is the mass flow factor, ζ_i is the Kronecker function, $\bar{u}$ and $\bar{\omega}$ are the dimensionless velocities, λ is the bearing coefficient.

Iteration method is applied to solve the finite element formula and the unknown nodes' pressures are obtained. Furthermore, properties of the aerostatic journal bearing, such as load capacity, attitude angle, volume flow rate and stiffness, can be calculated based on the obtained air film pressure (to study the calculation theory in detail, please refer to Liu *et al* [16]).

3.2. Computational domain

In this study, the computational domain of each aerostatic journal bearing is determined by half of the fluid zone which is symmetrical with respect to section a-a (section b-b for case 3). The meshed computational domain with right triangle elements and boundary conditions are illustrated in figure 2. Each orifice is regarded as a point in the domain and only one node is distributed to an orifice zone.

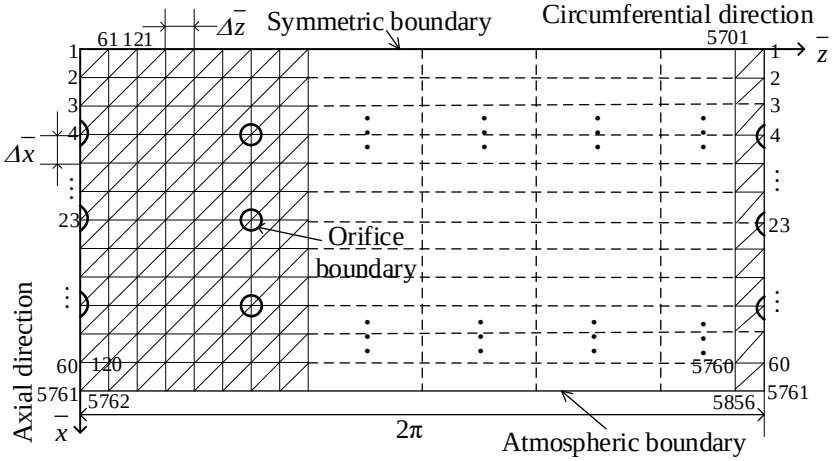

Figure 2. Meshes and boundary conditions of the computational domain (case 4).

Grid independence test is conducted to determine the computation grid size. Case 3 is chosen as the testing object. Two size schemes are scheduled as follows, scheme A is that the circumferential length of the bearing is equally cut into 96 parts in Z direction and the axial length is equally cut into 60 parts in X direction, producing 5856 nodes and 11520 triangular elements; Scheme B is that the circumferential length of the bearing is equally cut into 120 parts in Z direction and the axial length is equally cut into 60 parts in X direction, producing 7320 nodes and 14400 triangular elements. Rotational speed (n) of the bearing is 0 r/min, and the eccentricity ratios (ε) of the bearing is 0.3. The calculated load capacities and volume flow rates of the case 3 bearing are presented in table 1.

It can be found from table 1 that there are very small differences of the performance parameters between scheme A and scheme B. Besides, the grid quantity of scheme A is less than that of scheme B. Hence, scheme A is employed to mesh the computation domain.

Table 1. Load capacities and volume flow rates of two size schemes.

Parameters	Scheme A	Scheme B	$\frac{\text{Scheme A} - \text{Scheme B}}{\text{Scheme A}} \times 100\%$
Load capacity (N)	126.16	124.98	0.94%
Volume flow rate (L/min)	85.94	85.4	0.63%

3.3. Experimental verification

In order to verify the aforementioned analysing method, experimental results tested by Chen *et al* [9] are employed to this study. Air film stiffnesses of the bearings reported by Chen *et al* [9] are numerically analysed under condition of various supply pressures based on the proposed computational method. Table 2 presents the experimental and calculated results, indicating that the maximum difference between the experimental and calculated values is 10.02% which is acceptable for engineering purposes. Therefore, the proposed computational model is validated.

Table 2. Experimental [9] and calculated stiffnesses of aerostatic journal bearings.

Supply pressure (MPa)	Experimental (N/μm)	Calculated (N/μm)	Error (%)
Front bearing (L/D=1.5)			
0.6	10.1	11.038	-9.29
0.7	12.5	13.752	-10.02
0.8	16.2	16.903	-4.34
0.9	19.2	20.629	-7.44
Rear bearing (L/D=1.0)			
0.6	8.50	8.8733	-4.39
0.7	10.5	11.140	-6.10
0.8	13.6	13.836	-1.74
0.9	16.5	17.086	-3.55

4. Results and discussions

An analysing procedure is developed by MATLAB. The nonlinear equations are numerical solved by the 'fsolve' function with the termination tolerance of 1e-20. Pressure distribution, load capacity, attitude angle, volume flow rate and air film stiffness of four orifice layouts are thoroughly studied at various speeds and eccentricities.

Dimensionless air film pressure distributions of four orifice layouts under two running conditions (n=0 r/min, ε=0; n=200,000 r/min, ε=0.3) are shown in figure 3. It should be noted that the whole aerostatic journal bearing of case 3 is divided into two identical independent small aerostatic journal bearings and the dimensionless pressure distributions of each small aerostatic journal bearing are shown in figures 3(e) and 3(f). It can be found from figures 3(a), 3(c), 3(e) and 3(g) that an identical pressure value appears among twelve orifices of each orifice set along the circumferential direction when there is no eccentricity. Similar pressure profiles happen between case 1 and case 3, and the pressure distributions of case 2 and case 4 are also similar. What's more, the pressure uniformity decreases as in the sequence of cases of 4, 2, 1 and 3 under the same operating condition.

The load capacities of aerostatic journal bearings with four orifice layouts under working conditions of diverse rotational speeds and ε of 0.3 are described in figure 4. Figure 4 illustrates that load capacities of four orifice layouts increase as rotational speeds increased at ε of 0.3, and the load capacity of case 1 has the maximum growth rate. The load capacity of case 3 is the biggest one among four orifice layouts at rotational speeds from 0 r/min to 160,000 r/min, and the load capacity of case 1 becomes the largest one when the rotational speed is more than 170,000 r/min. Case 4 has the lowest load capacity at rotational speeds from 0 r/min to 200,000 r/min, and case 2 has the second lowest load

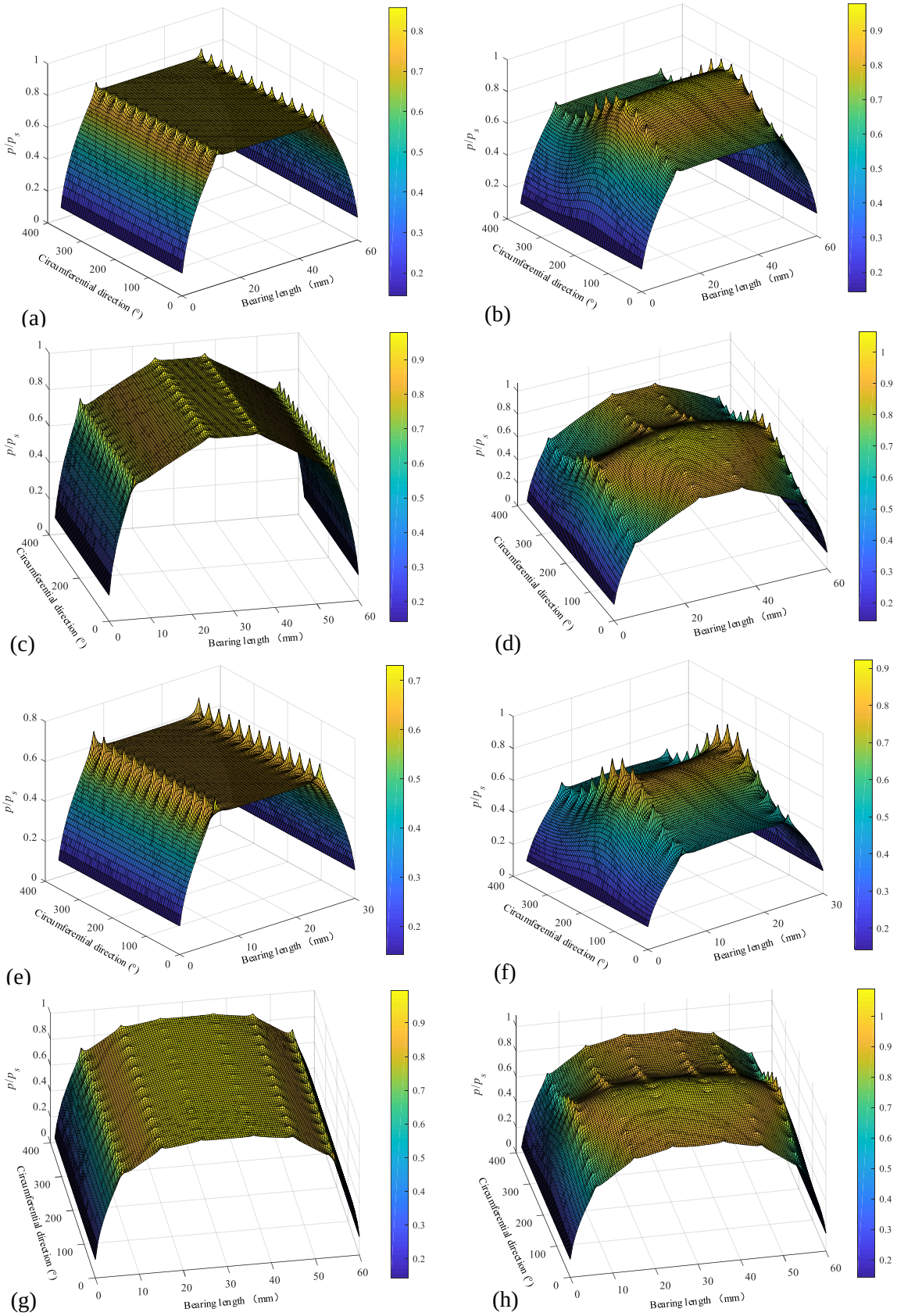

Figure 3. Dimensionless pressure profiles of four orifice layouts. (a) Case 1 (n=0r/min, ε=0). (b) Case

1 (n=200,000 r/min, ε=0.3). (c) Case 2 (n=0 r/min, ε=0). (d) Case 2 (n=200,000r/min, ε=0.3). (e) Case 3 (n=0 r/min, ε=0). (f) Case 3 (n=200,000 r/min, ε=0.3). (g) Case 4 (n=0r/min, ε=0). (h) Case 4 (n=200,000 r/min, ε=0.3).

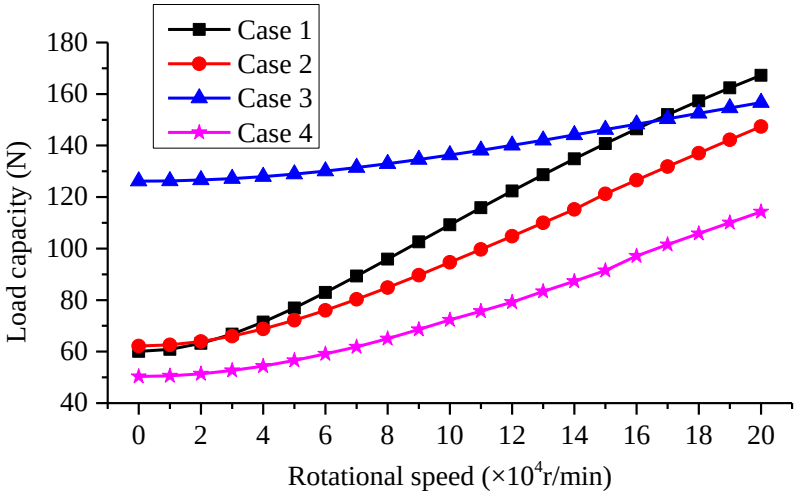

Figure 4. Load capacities of four orifice layouts with various rotational speeds.

capacity at rotational speeds from 30,000 r/min to 200,000 r/min. For cases 1, 2 and 4, the load capacity decreases with increasing orifice sets at speed of more than 20,000 r/min. Based on the aforementioned analysis, increasing orifice sets is not beneficial to increase the load capacity of the aerostatic journal bearing. However, the aerostatic journal bearing which is divided into two identical independent aerostatic journal bearings can greatly improve the load capacity at rotational speeds from 0 r/min to 160,000 r/min.

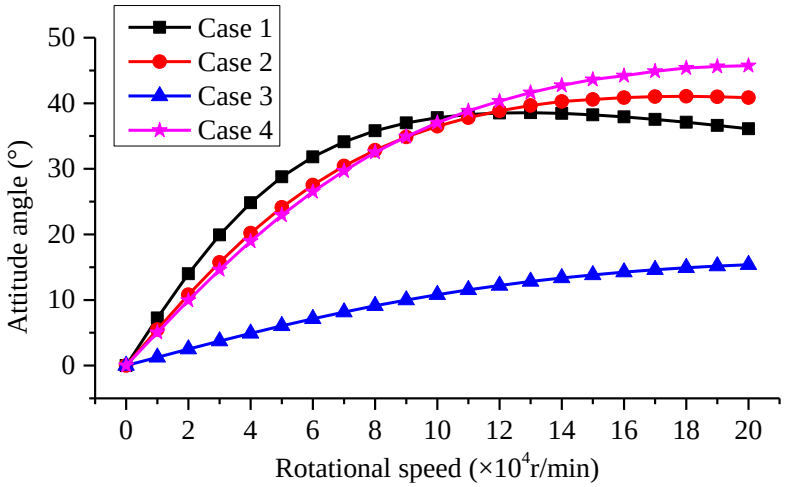

Figure 5. Attitude angles of four orifice layouts with various rotational speeds.

The attitude angles of aerostatic journal bearings with four orifice layouts under running conditions of diverse speeds and ε of 0.3 are shown in figure 5. It can be found from figure 5 that the attitude angles of case 1 and case 2 go up first and then they will go down with advancing speeds, and the attitude angles of case 3 and case 4 increase with increasing rotational speeds but the increasing rate is gradually slowed down. For cases 1, 2 and 4, the attitude angle increases with increasing orifice sets at speed of more than 110,000 r/min. However, case 3 has the lowest attitude angle at rotational speeds

from 0 r/min to 200,000 r/min, which means that case 3 has the lowest whirl force, presenting that case 3 has the best stability among four orifice layouts.

Volume flow rates of four orifice layouts at disparate speeds and ε of 0.3 are illustrated in figure 6. Figure 6 describes that the volume flow rates of four cases slowly decrease with increasing rotational speeds in general. For cases 1, 2 and 4, the volume flow rate increases with advancing orifice sets under identical operating conditions. The volume flow rate of case 3 is larger than those of other cases under the same operating conditions. The volume flow rates of four orifice layouts are ranked with sort descending under identical conditions, i.e. cases of 3, 4, 2 and 1. Based on the aforementioned analysis, the aerostatic journal bearing which is divided into two identical independent aerostatic journal bearings consumes the largest quantities of pressurized gas.

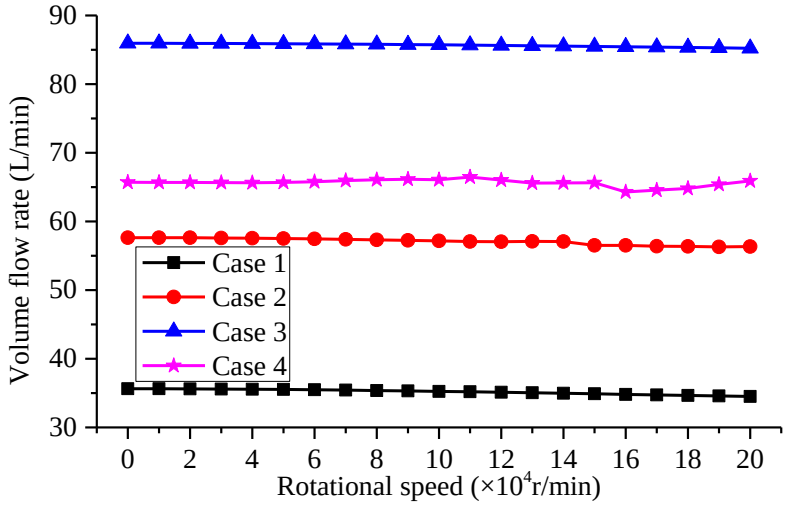

Figure 6. Volume flow rates of four orifice layouts with various rotational speeds.

Figure 7 depicts air film stiffnesses of four orifice layouts under conditions of various eccentricities and n of 200,000 r/min.

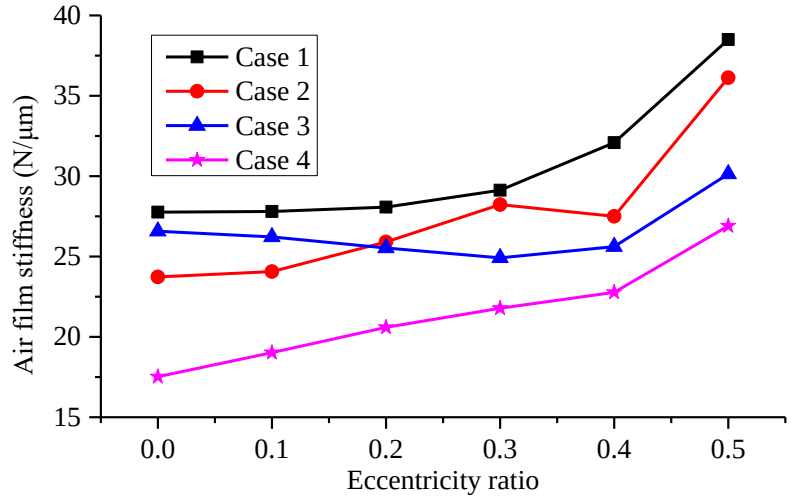

Figure 7. Air film stiffnesses of four orifice layouts with various eccentricity ratios.

As depicted in figure 7, it can be found that the air film stiffnesses of cases 1, 2 and 4 increase with increasing eccentricity ratios in general. Nevertheless, the air film stiffness of cases 3 decrease first

and then increase with increasing eccentricity ratios. For cases 1, 2 and 4, the air film stiffness decreases with increasing orifice sets under the same eccentricity ratios, presenting that increasing orifice sets cannot enhance the air film stiffness of the bearing. Eccentricity ratio of 0 is the point at which the bearing is firstly subjected to an external force. Hence, the air film stiffness at ε of 0 is the greatest important to the bearing among all air film stiffnesses. The difference is 4.27% between the air film stiffnesses of case 1 and case 3 at ε of 0, which can be ignored, presenting that the air film stiffness of case 3 is acceptable for engineering purposes with respect to that of case 1.

5. Conclusions

This paper investigated influences of various orifice layouts on properties of the aerostatic journal bearing by numerically solving the Reynolds equation based on FEM, and air film pressure, bearing load capacity, bearing attitude angle, bearing volume flow rate and air film stiffness of four different orifice layouts are analyzed under different operating conditions. Based on the aforementioned analysis results of four orifice layouts, it can be concluded that increasing orifice sets is not beneficial to strengthen abilities of aerostatic journal bearings. Aerostatic journal bearing which is divided into two identical independent aerostatic journal bearings (case 3) has the relative optimal performance, the highest load capacity, the lowest attitude angle and modest air film stiffness, at rotational speeds from 0 r/min to 160,000 r/min. However, the case 3 bearing consumes the largest quantities of pressurized gas. Based on the obtained analysis results, engineers can better design the orifice layout for higher precision aerostatic journal bearing with a large length-diameter ratio.

Acknowledgments

The authors thank for the funding support for this research by the State Key Laboratory of Mechanical Transmissions (Grant No. SKLMT-KFKT-201801), the National Natural Science Foundation of China (Grant No. 51705501, 51705500), the CASHIPS Director's Fund (Grant No. YZJJ201622) and the State Key Lab of Digital Manufacturing Equipment and Technology in China (Grant No. DMETKF2017017).

References

[1] Stanev P T, Wardle F and Corbett J 2004 Investigation of grooved hybrid air bearing performance *P. I. Mech. Eng. K.-J. Mul.* **218** 95-106
[2] Gao Q, Chen W, Lu L, Huo D and Cheng K 2019 Aerostatic bearings design and analysis with the application to precision engineering: State-of-the-art and future perspectives *Tribol. Int.* **135** 1-17
[3] Abele E, Altintas Y and Brecher C 2010 Machine tool spindle units *CIRP. Ann.-Manuf. Techn.* **59** 781-802
[4] Cheng K and Huo D 2013 *Micro Cutting: Fundamentals and Applications* (West Sussex: Wiley)
[5] Lo C Y, Wang C C and Lee Y H 2005 Performance analysis of high-speed spindle aerostatic bearings *Tribol. Int.* **38** 5-14
[6] Su J C T and Lie K N 2003 Rotation effects on hybrid air journal bearings *Tribol. Int.* **36** 717-26
[7] Xiao H, Li W, Zhou Z, Huang X and Ren Y 2018 Performance analysis of aerostatic journal micro-bearing and its application to high-speed precision micro-spindles *Tribol. Int.* **120** 476-90
[8] Liu Z S, Zhang G H and Xu H J 2009 Performance analysis of rotating externally pressurized air bearings *P. I. Mech. Eng. J.-J. Eng.* **223** 653-63
[9] Chen Y S, Chiu C C and Cheng Y D 2010 Influences of operational conditions and geometric parameters on the stiffness of aerostatic journal bearings *Precis. Eng.* **34** 722-34
[10] Belforte G, Colombo F, Raparelli T, Trivella A and Viktorov V 2011 Comparison between grooved and plane aerostatic thrust bearings: static performance *Meccanica* **46** 547-55
[11] Belforte G, Colombo F, Raparelli T, Trivella A and Viktorov V 2008 High-speed electrospindle

running on air bearings: design and experimental verification *Meccanica* **43** 591-600
[12] Zhang G and Ehmann K F 2015 Dynamic design methodology of high speed micro-spindles for micro/meso-scale machine tools *Int. J. Adv. Manuf. Tech.* **76** 229-46
[13] Yao Y X, Qin D L and Zhang H B 2006 Static performance analysis of orifice compensated externally pressurized gas spherical bearing based on FEM *Key. Eng. Mater.* **315-316** 860-3
[14] Du J, Zhang G, Liu T and To S 2014 Improvement on load performance of externally pressurized gas journal bearings by opening pressure-equalizing grooves *Tribol. Int.* **73** 156-66
[15] Gao S, Cheng K, Chen S, Ding H and Fu H 2017 Computational design and analysis of aerostatic journal bearings with application to ultra-high speed spindles *P. I. Mech. Eng. C.-J. Mec.***231** 1205-20
[16] Liu T, Liu Y H and Chen S J 1990 *Aerostatic Lubrication* (Harbin: Press of Harbin Institute of Technology)